An all-composite, all-electric, morphing trailing edge device for flight control on a blended-wing-body airliner

A Wildschek[1]*, **T Havar**[1], and **K Plötner**[2]
[1]EADS Innovation Works, Munich, Germany
[2]Technische Universität München, Institute for Aeronautics and Lightweight Structures, Garching, Germany

The manuscript was received on 14 May 2009 and was accepted after revision for publication on 10 August 2009.

DOI: 10.1243/09544100JAERO622

Abstract: For a significant improvement in the fuel efficiency of long-range transport aircraft, a transition to blended-wing-body (BWB) configurations will be required in the long term. Further efficiency improvements are expected from an all-composite primary structure, all-electric actuation, as well as from seamless control surfaces that provide reduced drag compared to conventional control surfaces. BWB configurations feature specific demands on the control system because of the high coupling between flap deflections and aircraft movements in all three axes. Thus, multi-objective control surfaces are required for flight control, as well as for active gust and manoeuvre load alleviation. A major challenge therefore is to provide sufficient yaw control and stability in the absence of a vertical tail. Generally, one engine inoperative poses an important sizing case for the control system design, especially for the control surfaces.

In this article, the sizing of winglet flaps and crocodile flaps is performed for the preliminary design of an all-composite, all-electric BWB airliner. For further improvement in efficiency, a seamless morphing trailing edge device is designed that provides both crocodile flap and aileron modes at the same time. Based on these results, a composite morphing trailing edge demonstrator with an all-electric actuation system is investigated. Some open issues remain for investigation. Still, the proposed design provides a promising approach for further efficiency improvement on BWB aircraft configurations.

Keywords: blended-wing-body, yaw stability, yaw control, morphing trailing edge, crocodile flap

1 INTRODUCTION

For the realization of future ultra-efficient long-range airliners, various configurational changes have been proposed so far. In reference [**1**] the design of blended-wing-body (BWB) subsonic civil transport aircraft is presented. Also, regarding environmental considerations, BWB configurations provide many advantages such as a low noise signature [**2**]. The highest fuel efficiency is expected from tailless configurations.

Because of the high coupling between flap deflections and aircraft movements, multi-objective control surfaces are required for flight control, as well as for active gust and manoeuvre load alleviation. The mentioned characteristics pose new challenges not only for the control law design, but also for the control surface concept. One major problem related to BWB configurations is yaw stability and control, especially in the case of one engine inoperative (OEI).

This case has been identified as a dominant criterion for the presizing of yaw control devices for the preliminary design of a BWB airliner with two top-rear high-bypass turbo fan engines and winglets. For the presented configuration, the usage of winglets as the only source for yaw control could be demonstrated as being insufficient for handling the OEI case. This is mainly due to winglet size limitations in regard to flutter in cruise. Hence, additional control devices for yaw control and stability (i.e. crocodile flaps) are introduced in order to fulfil the basic OEI certification criterion of yaw moment equilibration in the OEI case.

*Corresponding author: EADS Innovation Works, Willy-Messerschmitt-Str. 1, Munich, D-81663, Germany.
email: Andreas.Wildschek@EADS.net

2 YAW CONTROL ON A BWB CONFIGURATION

On tailless BWB configurations, not only winglet flaps but also crocodile flaps are required on the outboard wings for yaw stability and control as will be shown in the following. Since this area of the trailing edge is also required for the (low-speed) ailerons, an outboard trailing edge flap design is aspired that provides both crocodile flap and aileron modes at the same time.

In order to meet this demand, the design of a multi-functional control surface is investigated for a future BWB airliner. As illustrated in Fig. 1, such a control surface concept can be used for roll (i.e. $C_{L_{LW}} \neq C_{L_{RW}}$) and yaw (i.e. $C_{D_{LW}} \neq C_{D_{RW}}$) at the same time. Moreover, the proposed flap device provides an airbrake mode (i.e. for $C_{D_{LW}} = C_{D_{RW}}$).

The dimensioning case for the preliminary sizing of yaw control devices of airliners is generally the OEI case during take-off and landing. In Fig. 2, the acting forces are outlined for a future BWB airliner with two top-rear turbo fan engines, winglets, and crocodile flaps in order to explain the dimensioning of yaw control devices for yaw stabilization in the OEI case (in Fig. 2, the right engine is inoperative).

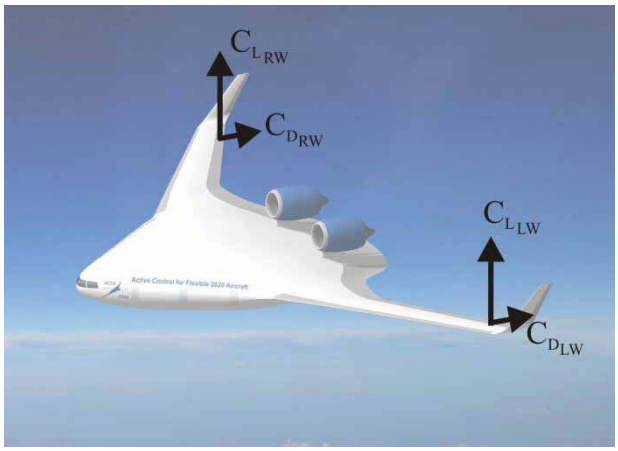

Fig. 1 BWB airliner (courtesy of the ACFA Consortium)

In order to ensure lateral control and thus fulfil the certification requirements for the OEI case, the sum of all yaw moments at the centre of gravity (CG) must be zero

$$N = N_{\mathrm{OEI}} + N_{\mathrm{OEO}} - N_{\mathrm{BWB}} - 2N_{\mathrm{winglet}} - N_{\mathrm{crocodile\ flaps}} \tag{1}$$

In Fig. 2, the right engine is assumed to be inoperative and produces (due to the wind-milling effect) a drag force $F_{x,\mathrm{OEI}}$, whereas the left engine generates maximum available thrust $F_{x,\mathrm{OEO}}$. In a first assumption, the available remaining thrust of the operative engine is sufficient to ensure the required climb gradient during take-off. The lateral position of the engines y_{e} relative to the CG induces the yaw moments N_{OEI} (one engine inoperative) and N_{OEO} (one engine operative)

$$N_{\mathrm{OEO}} = F_{x,\mathrm{OEO}}\, y_{\mathrm{e}} \tag{2}$$

$$N_{\mathrm{OEI}} = F_{x,\mathrm{OEI}}\, y_{\mathrm{e}} = N_{\mathrm{OEO}}\, k \tag{3}$$

with k denoting the wind-milling coefficient for turbo fan engines. Values for k can be obtained from references [**3**] and [**4**].

The yaw moment only due to a single winglet rudder deflection, i.e. N_{winglet}, can be calculated as follows

$$N_{\mathrm{winglet}} = x_{\mathrm{winglet}}\, F_{\mathrm{y,winglet}} = (x_{\mathrm{ac,winglet}} - x_{\mathrm{cg}}) \times q\, A_{\mathrm{winglet}}\, C_{\mathrm{L,winglet}} \tag{4}$$

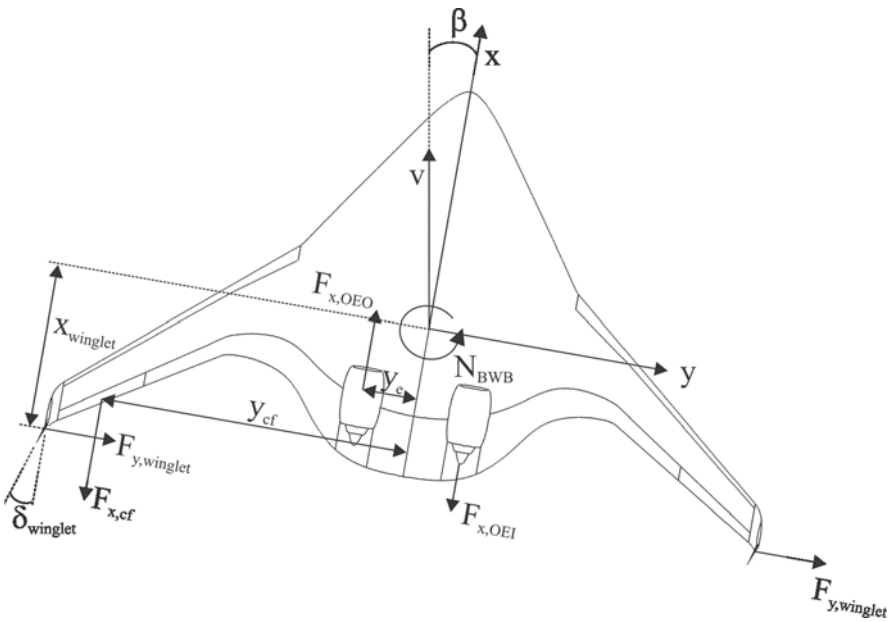

Fig. 2 Acting forces on a BWB configuration in OEI flight condition

$$C_{\mathrm{L,winglet}} = C_{\mathrm{L}\delta,\mathrm{winglet}}\ \delta_{\mathrm{winglet}}\ K' \tag{5}$$

$$C_{\mathrm{L}\delta,\mathrm{winglet}} = 1.2\ C_{\mathrm{L}\alpha,\mathrm{winglet}}\ K_{\mathrm{b}} \sqrt{\frac{l_{\mathrm{r}}}{l}} \tag{6}$$

The winglet rudder deflection yaw moment N_{winglet} is generated by the side force $F_{y,\mathrm{winglet}}$ depending on the incremental lift coefficient $C_{\mathrm{L,winglet}}$, the dynamic pressure q, and the winglet area A_{winglet}. The incremental lift coefficient $C_{\mathrm{L,winglet}}$ can be calculated from the lift gradient due to a rudder deflection $C_{\mathrm{L}\delta,\mathrm{winglet}}$, the rudder deflection angle $\delta_{\mathrm{winglet}}$, and a rudder effectiveness parameter K' that depends on the ratio of the rudder chord to the winglet chord, as well as on the rudder deflection angle $\delta_{\mathrm{winglet}}$ [**5**]. $C_{\mathrm{L}\delta,\mathrm{winglet}}$ depends on the lift curve slope $C_{\mathrm{L}\alpha,\mathrm{winglet}}$ of the entire winglet, the ratio of rudder chord l_{r} to local winglet chord l and a rudder-span factor K_{b} [**6**] taking into account the rudder's position at the winglet along the Z-axis.

For the negative sideslip angle β illustrated in Fig. 2, a wing-body configuration generates a positive (destabilizing) yaw moment, which has to be counterbalanced, e.g. by vertical tails. For BWB aircraft configurations with slender transition between the centre body and the outer wing and neglecting the winglets, installed engines and pylons, a neutral yaw moment derivative can be assumed. With winglets and installed top-rear engines, the yaw moment derivative of the above shown configuration becomes positive and generates a counterbalancing yaw moment N_{BWB} (see Fig. 2).

As indicated by Fig. 2, it can be shown that for the BWB in the OEI case, the yaw moments induced by the two engines cannot be compensated for by the winglet alone. With a fixed winglet taper ratio, the winglet size is limited in height and hence in total winglet area, mainly due to flutter constraints of the outer wing and the winglet in cruise condition. For the remaining yaw moment that has to be counterbalanced by other devices, crocodile flaps were chosen as an effective means for yaw stabilization. The yaw is generated by deflecting either the left or the right crocodile flap. The resulting yaw moment due to a crocodile flap deflection can be calculated as follows

$$N_{\mathrm{crocodile\ flaps}} = y_{\mathrm{cf}}\ F_{x,\mathrm{cf}} = y_{\mathrm{ac,cf}}\ q\ A_{\mathrm{ref}}\ C_{\mathrm{D,cf}} \tag{7}$$

$$C_{\mathrm{D,cf}} = 0.5\ C_{\mathrm{d,cf}}\ \frac{A_{\mathrm{cf}}}{A_{\mathrm{ref}}} \tag{8}$$

$$C_{\mathrm{d,cf}} = C_{\mathrm{d}\delta,\mathrm{cf}}\ \delta_{\mathrm{cf}} \tag{9}$$

A_{cf} represents the wing-affected flap area and A_{ref} the BWB's reference area. The airfoil drag coefficient for a crocodile flap deflection of $\delta_{\mathrm{cf}} = 30°$ can be taken from reference [**7**]. This value is then used for sizing of the crocodile flaps in order to provide yaw moment equilibration in the OEI case. For the BWB configuration shown above, crocodile flaps were sized with a flap chord of 24 per cent of the wing chord and span from 75 per cent of the BWB half span to 97 per cent of the BWB half span.

3 THE MORPHING TRAILING EDGE CONCEPT

In order to minimize the drag in the aileron mode, a design without span-wise gaps between the flap and the wing is preferred. Thus, a seamless (morphing) trailing edge device was considered for the BWB aircraft. The following specifications were imposed.

1. A large range of deflection angles for sufficiently high maximum yaw and roll moment.
2. Aileron function for roll (i.e. $C_{\mathrm{L_{LW}}} \neq C_{\mathrm{L_{RW}}}$), which can also be used for pitch.
3. Crocodile flap function for yaw control (i.e. $C_{\mathrm{D_{LW}}} \neq C_{\mathrm{D_{RW}}}$) and airbrake mode (i.e. $C_{\mathrm{D_{LW}}} = C_{\mathrm{D_{RW}}}$).

The additional constraints were that a carbon fibre structure is to be used, as well as an electro-mechanic actuation system, i.e. a ball screw or a roller screw, e.g. a planetary roller screw featuring high force capability at low volume. The seamless outer surface is achieved by splitting the trailing edge of the wing into an upper and a lower morphing control surface as described in references [**8**] to [**10**] (see Fig. 3). With this concept, an (upper and lower) inner structure is moved by electric actuators. This inner structure is hinged to stringers that are bonded to the upper and lower outer skins. This allows the transmission of moments M into the outer skins, enhancing the deformation of the flap. The (position-dependent) bending moments M and thus the curvature of the deflected surface can be adjusted by the stiffness of the stringers (i.e. design parameters.)

By actuating the upper and the lower inner structure in opposite directions the trailing edge is simply deflected (i.e. aileron mode with $\eta = \eta_{\mathrm{upper}} = \eta_{\mathrm{lower}}$). Thereby, the upper and lower control surfaces are pressed against each other by design so that the split remains tightly closed. The crocodile flap mode is obtained by actuating the upper and the lower inner structure in the same direction (i.e. $\eta_{\mathrm{upper}} = -\eta_{\mathrm{lower}}$). In order to be able to combine those two modes, both the upper and the lower inner structure can be activated separately.

The transformation of roll and yaw commands to the commands on the actuators of the upper and the lower inner structure has to be achieved by control law design. Due to three-dimensional (3D) effects (i.e. due to the twist, sweep and taper ratio of the wings), the actuator force and displacement required for a flap deflection are span dependent. Thus, several span-wise distributed screw actuators (see for example of different sizes) are envisaged, which also helps in supporting the highly flexible trailing edge device in the span-wise direction. In this context, it has to be mentioned that the fail-safe behaviour/failure management (see for example in case of jam of the mechanical

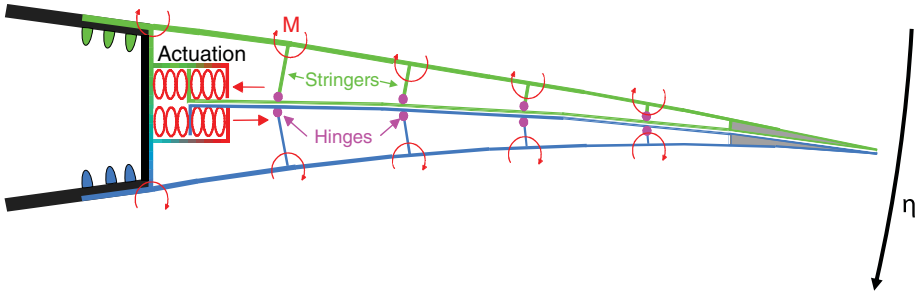

Fig. 3 The morphing trailing edge concept

drive trains, failure behaviour of the electric motors, etc.) still needs to be investigated.

4 THE MORPHING TRAILING EDGE DESIGN

The structure of the morphing trailing edge device consists of composite outer skin layers and stringers and inner middle skins as already shown in Fig. 3. On the one hand, the outer skins need to be deformable in order to achieve required flap deflections, but on the other hand they need to have a sufficient stiffness in order to prevent lateral deformations under cruise air loads.

In this context, composite materials show great potential due to the ability to adjust the stiffness independently in different directions. These characteristics can be used in order to increase the stiffness in the span direction of the morphing flap's skin but to decrease the stiffness in the chord direction, allowing for a span-wise smooth deflection of the trailing edge while minimizing actuation loads.

Composites also show high static strengths as well as high allowable strains of up to 1 per cent, as illustrated in Fig. 4. The implementation of composites for the morphing flaps' skins thus enables high deflection angles without early failure or fractures of the skins. Figure 4 compares different epoxy and thermoplastic composite aerospace materials in regard to their yield strain at certain fibre angles. The solid lines represent the average yield strain and the dashed lines correspond to yield strains that are used for the sizing of composite structures including knock down factors for material tolerances and environmental conditions. Glass-fibre reinforced plastic epoxy composites have the highest allowable strain in the fibre direction, due

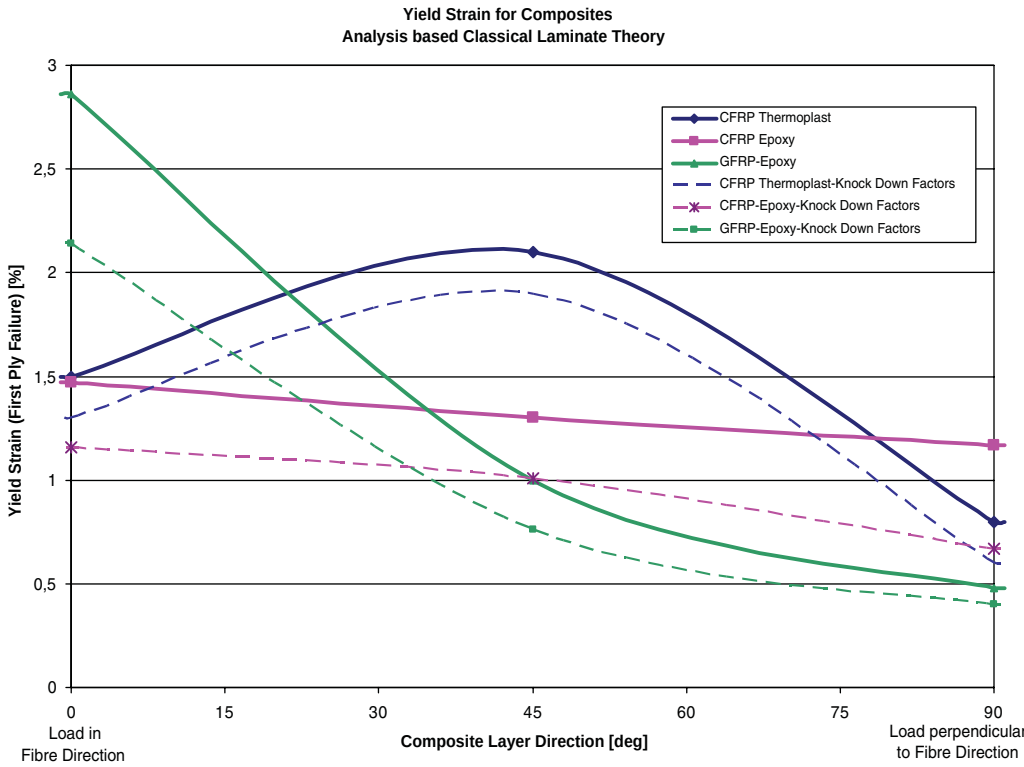

Fig. 4 Allowable strains for different aerospace composites

to their high tensile strength and low stiffness. Carbon-fibre reinforced plastic (CFRP) composites with a thermoplastic matrix show the best performance in other tension directions than the fibre direction. For an optimal morphing trailing edge design hence, CFRP thermoplastic composites are used.

The use of the morphing trailing edge device as an aileron will result in 100 000–1 000 000 load cycles for the flap structure based on an average aircraft life cycle. Although composite materials generally have good fatigue behaviour and are consequently predestined for application to such a morphing structure, the issue of fatigue of the proposed (safety critical) morphing trailing edge device needs to be investigated.

The wing loading with maximum payload at 1 g cruise is about $\bar{p}_{\text{nom}} = 290\,\text{kg/m}^2$ for the BWB predesign. A simplified distribution of deflection-independent aerodynamic pressure p over the normalized flap chord is illustrated in Fig. 5. Thereby, the aerodynamic pressure p is related to the mean static pressure on the crocodile flap $\bar{p}_{\text{cf}}$. The distribution represents the resulting pressure from the suction on the upper wing surface, and the overpressure on the lower wing surface. For simplicity, suction and overpressure are each considered to contribute 50 per cent to the total pressure.

For the structural predesign of the morphing trailing edge device, two load cases are considered in order to compute a mean static pressure $\bar{p}_{\text{ref}}$ for the whole BWB.

1. Loads for static strength: 2.5 g (gust or manoeuvre) with the maximum payload under which the aircraft structure must only avoid collapsing. For this load case, the usual security factor of 1.5 has been considered.
2. Loads for stiffness design: 1 g with maximum payload.

Two effects have to be considered in order to obtain a realistic mean pressure on the morphing trailing edge device. On the one hand, the pressure is higher on the wing than on the fuselage body on a BWB in order to achieve an elliptic lift distribution. On the other hand, the pressure on the morphing device is increased when it is deflected. An admittedly oversimplified approach for the estimation of the static pressure $\bar{p}_{\text{cf}}$ to be considered for the structural predesign of the trailing edge device is to just multiply $\bar{p}_{\text{ref}}$ by a factor that considers these two effects.

For a representative wing cross-section, a 2D morphing trailing edge device with a 750 mm chord was designed. Deformations of the morphing part of the profile under 1 g cruise condition with maximum payload were computed by numeric analysis (see Fig. 6). The trailing edge was modelled with ANSYS with 2D elements and orthotropic material definitions. The aerodynamic loads were applied to the upper and lower skins. In a first step, the composite skins were designed for high trailing deflection leading to high skin thicknesses with mainly 0° fibres at the front and thin skin thickness with a quasi-isotropic lay-up at the trailing edge. Afterwards, the morphing structure was analysed against aerodynamic loading. In the first load case, the actuators were locked, and at a second load case, they were deflected to compensate for the deflection at the trailing edge. The internal loading and the deflection were calculated with linear analysis.

At the first load case (locked actuators), the resulting deflection at the trailing edge is 0.69 mm, but the largest deformation is further upfront at about 2/3 of the morphing structure (Fig. 5). Therefore the maximum vertical deformation of the morphing device is 11.6 mm, represented by a small bump. The bump is a result of the required flexibility of the skins, which in turn is needed in order to be able to deflect the morphing trailing edge device. In Fig. 6, the dashed lines represent the morphing structure without aerodynamic loading and the continuous lines represent the morphing structure with aerodynamic load as specified.

At the second load case where the vertical displacement at the trailing edge was compensated for by the actuators, the maximum displacement increased at the bump to 14.4 mm. This leads to a larger aerodynamic disadvantage and is therefore not considered further.

The undesirable bump can be compensated for by manufacturing skins that are slightly curved (predeformed) in the opposite direction (see Fig. 7).

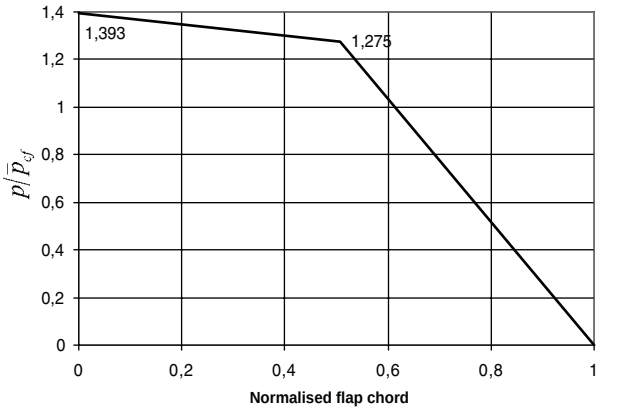

Fig. 5 Pressure distribution over the normalized flap chord

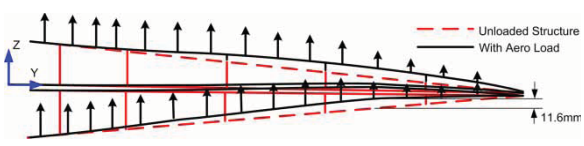

Fig. 6 Deformation of the morphing trailing edge device due to aerodynamic loading

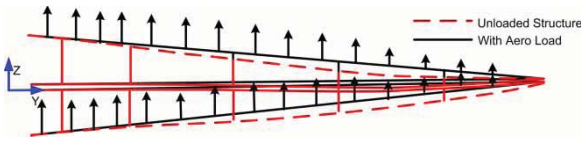

Fig. 7 Precurved morphing trailing edge device under aerodynamic loading

This approach would allow for a nearly undeformed wing profile for 1 g cruise condition. For other flight conditions such as take-off and landing, the morphing device would still feature the undesirable bump.

Numeric analysis was also used for the computation of the required actuator force per unit length F in kN/m against vertical displacement d for one trailing edge half, i.e. the upper or lower side, respectively (see Fig. 8). With the oversimplified consideration of deflection-independent aerodynamic forces that was introduced above, one can see that the vertical trailing edge displacement is still a slightly non-linear function of the actuator force. This non-linearity is thus solely due to the stiffness of the morphing structure. It could be shown by numerical analysis that, for $F = 30\,\text{kN/m}$ (respectively $d = 480\,\text{mm}$), the strains remain within controllable limits and the morphing structure is still secure against buckling.

With a local crocodile flap chord of $c_{\text{cf}} = 600\,\text{mm}$ (obtained by definition of an equivalent flap pivotal point) the vertical trailing edge displacement d can be converted to an equivalent deflection angle η (for aileron mode) or δ_{cf} (for crocodile flap mode), respectively

$$\delta_{\text{cf}} = \arctan \frac{d}{c_{\text{cf}}} [\text{rad}] \tag{10}$$

Making use of this conversion, Fig. 9 shows the required actuator force per unit length F in kN/m against the equivalent deflection angle δ_{cf} in degrees. It can be seen that the proposed morphing trailing edge device provides more than 35° maximum deflection angle, which is sufficient for yaw control authority in the OEI case. It needs to be checked, however, whether the remaining control authority for roll control (also including the use of all other trailing edge devices such as the flaps inboard the morphing trailing edge device) is sufficient with the $\delta_{\text{cf}} = 30°$ required for yaw moment compensation in the OEI case, compare section 2.

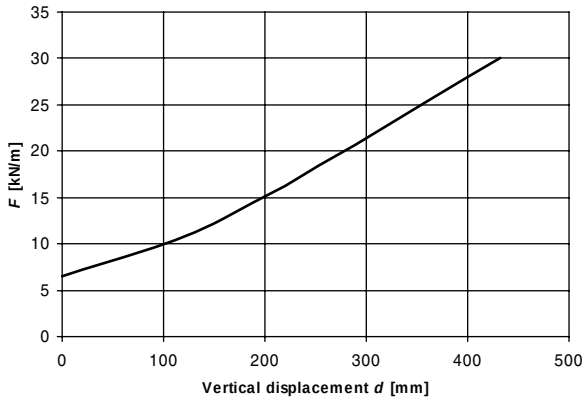

Fig. 8 Required actuator force against vertical trailing edge displacement

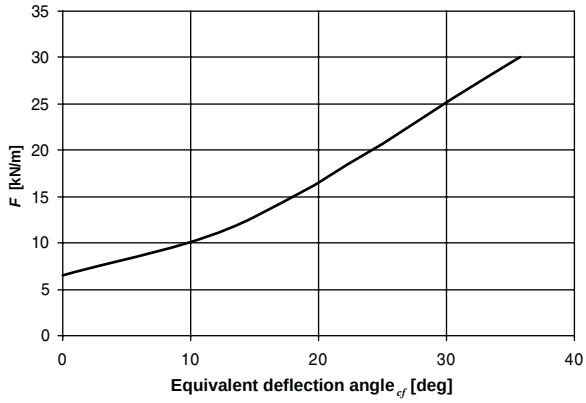

Fig. 9 Required actuator force against equivalent deflection angle

The maximum actuator force per unit length of $F = 30\,\text{kN/m}$ obtained from Figs 8 or 9, respectively, can be used for subsequent predesign of the span-wise distributed electro-mechanic actuators.

In order to demonstrate the functionality of the proposed morphing trailing edge device, a 2D wing segment of 350 mm span width was built. For roll control on the BWB airliner (i.e. $C_{\text{L}_{\text{LW}}} \neq C_{\text{L}_{\text{RW}}}$), the aileron mode is required (i.e. $\eta = \eta_{\text{upper}} = \eta_{\text{lower}}$) (see Fig. 10). This mode can also be used for pitch control.

For yaw moment equilibration in the OEI case, or cross wind landing (i.e. requirement of $C_{\text{D}_{\text{LW}}} \neq C_{\text{D}_{\text{RW}}}$), as well as for the airbrake mode (i.e. requirement of

Fig. 10 Aileron mode for roll and pitch control

Fig. 11 Crocodile flap mode for yaw control and air brake function

$C_{D_{LW}} = C_{D_{RW}}$) the crocodile flap function is used (i.e. $\delta_{cf} = \eta_{upper} = -\eta_{lower}$) (see Fig. 11).

5 CONCLUSIONS AND PERSPECTIVE

Based on the predesign of a large BWB airliner, a method for the preliminary design of the crocodile flaps used for yaw moment equilibration in the OEI case has been introduced. For maximum effectiveness, the crocodile flaps have to be placed as far outboard as possible, i.e. at the same position where the (low-speed) ailerons should be placed. Thus, a multi-objective trailing edge device is aspired, which provides aileron and crocodile flap function at the same time. Since the crocodile flap is only opened in selected flight situations (such as cross wind landing, or the OEI case), the device is supposed to work as a conventional aileron in normal flight operation. In order to minimize the drag in the aileron mode, a wing design without span-wise gaps between the flap and the wing is preferred. Thus, a seamless (morphing) trailing edge device was considered for the BWB aircraft. The morphing device thereby has to provide a sufficiently large range of deflection angles in both aileron and crocodile flap modes for sufficient aircraft control authority, even in the OEI case.

These design goals are achieved by splitting the trailing edge of the outer wing into an upper and a lower morphing control surface that can be actuated independently. For demonstration purposes, a 2D wing segment including such a morphing control surface was designed. The investigated morphing structure shows a good design approach with the capacity for high deflections and high static strengths. These properties are realized with composite skins, which enable high deflections by offering high bending capabilities. The lay-up of these composite skins can be further optimized for a smooth span-wise trailing edge deflection with smaller actuation loads. The

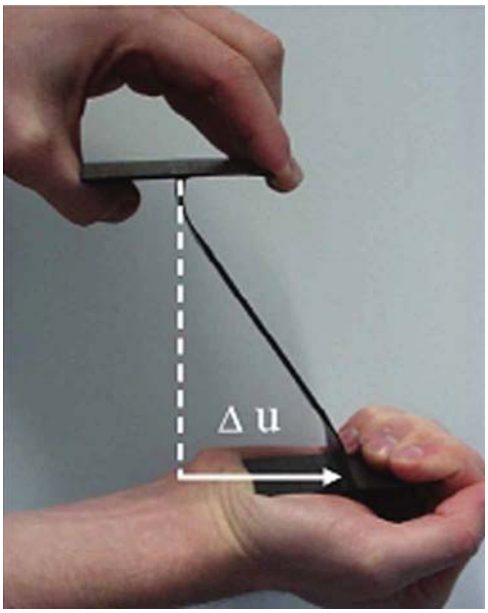

Fig. 12 Flexible spar

Fig. 13 Hinge-spars

stringers are currently connected to the inner composite skins by aluminium fittings with small hinges. This preliminary design demonstrates the feasibility of the proposed morphing control surface, but a high potential remains in regard to fatigue and maintenance. Further investigations related to morphing aircraft structures have been performed for flexible composite spars [**11**] (see Fig. 12), as well as with hinged composite spar attachments (see Fig. 13). These investigations show good fatigue behaviour of flexible spars for small shear deflections as shown in Fig. 12. For large shear deformations, however, spar attachments with integrated composite hinges show a better performance (see Fig. 13).

These approaches for deformable spars show great potential and should be investigated for the proposed morphing trailing edge device in the future, enabling a robust and lightweight design. Moreover, issues such as the fail-safe behaviour, especially in regard to the

actuator design, need to be considered in subsequent research activities.

In general, it can be said that the proposed morphing trailing edge concept has a high potential for realizing adaptive wing structures. The feasibility of the proposed morphing trailing edge concept is shown, but a lot of work remains to be done, especially in regard to the assessment of functional capabilities under real mission conditions. The structure is loaded to its limits in order to fulfil the required aerodynamic performance. The concept can be demonstrated at the laboratory level, but in real mission conditions this high loading would probably lead to early failures. The fatigue and damage tolerance performance of the morphing trailing edge therefore needs to be improved in order to be able to implement the trailing edge concept for a flying aircraft. Additionally, impact scenarios still have to be investigated as for any primary aircraft structures. The technology readiness level of the proposed morphing trailing edge concept, however, is comparable to the one of the predesigned BWB airliner.

ACKNOWLEDGEMENTS

The authors would like to thank the European Commission for funding the ACFA2020 (Active Control for Flexible 2020 Aircraft) project within the Seventh Research Framework Programme. Many thanks also go to all ACFA2020 partners for their contributions. Moreover, the authors are grateful to Günther Müller and Josef Steigenberger for their long-time research on morphing wing structures and for the design of the morphing trailing edge demonstrator.

REFERENCES

1 **Liebeck, R.** Design of the blended-wing-body subsonic. In Proceedings of the Transport 40th AIAA Aerospace Sciences Meeting and Exhibit, Reno, NV, 14–17 January 2002.
2 **Hileman, J., Spakovsky, Z., Drela, M.,** and **Sargeant, M.** Airframe design for silent aircraft. AIAA paper 2007-0453, 2007.
3 **Raymer, D.** *Aircraft design: a conceptual approach* (AIAA Education Series), 3rd edition, 1999, p. 651 (AIAA, USA).
4 **Scholz, D.** *Flugzeugentwurf, Skript zur Vorlesung Flugzeugentwurf*, Hamburg University of Applied Sciences, Hamburg, Germany, 1999, p. 228.
5 **Hoak, D. E.** USAF Stability and Control Datcom, 1969, USA, Fig. 6.1.1.1–26.
6 **Hoak, D. E.** USAF Stability and Control Datcom, 1969, USA, Fig. 6.1.4.1–9.
7 **Purser, P. E.** Wind-tunnel investigation of perforated split flaps for use as dive brakes on rectengular NACA 23012 airfoil. NACA report, Washington, USA, Fig. 27, 1941.
8 *Adaptive body flow*. United States Pat. US6276641.
9 **Müller, G., Grünewald, M., Möser, C.,** and **Steigenberger, J.** Variable Flügelstruktur – Auftriebsanpassung, Widerstandsreduzierung. In Proceedings of the Jahrbuch 1999 der Deutschen Gesellschaft für Luft- und Raumfahrt – DGLR Jahrbuch, Bonn, 1999, vol. 1, pp. 13–18.
10 **Wildschek, A., Grünewald, M., Maier, M., Steigenberger, J., Judas, M., Deligiannidis, N.,** and **Aversa, N.** Multifunctional morphing trailing edge device for control of all-composite, all-electric flying wing aircraft. In Proceedings of the 26th Congress of International Council of the Aeronautical Science, including the Eighth AIAA Aviation Technology, Integration, and Operations Conference, Anchorage, Alaska, 14–19 September 2008.
11 **Bauer, C.** *Die rippenlose Wölbklappe*, 2000 (Shaker Verlag, Germany).

APPENDIX

Notation

A_{cf}	crocodile flap area
A_{ref}	wing reference area
$A_{winglet}$	winglet area
BWB	blended-wing-body
c_{cf}	local crocodile flap chord/equivalent crocodile flap chord of the demonstrator
$C_{d,cf}$	drag coefficient due to crocodile flap deflection
$C_{d\delta,cf}$	drag lift curve slope due to crocodile flap deflection
$C_{D,cf}$	configuration's drag coefficient due to crocodile flap deflection
$C_{D_{LW}}$	drag coefficient of the left wing due to crocodile flap deflection
$C_{D_{RW}}$	drag coefficient of the right wing due to crocodile flap deflection
CG	centre of gravity
$C_{L_{LW}}$	lift coefficient of the left wing
$C_{L_{RW}}$	lift coefficient of the right wing
$C_{L\alpha,winglet}$	lift curve slope of winglet
$C_{L\delta,winglet}$	lift coefficient of winglet due to rudder deflection
$C_{L,winglet}$	lift coefficient of winglet
d	vertical displacement of the flap's trailing edge
F	actuator force required for the deflection of one trailing edge half
$F_{x,cf}$	aerodynamic force due to crocodile flap deflection
$F_{x,OEI}$	drag of inoperative engine
$F_{x,OEO}$	take-off thrust of operative engine
$F_{y,winglet}$	aerodynamic force due to winglet rudder deflection
F_0	static actuator force required for zero-deflected trailing edge in 1 g cruise with maximum payload

k	wind-milling factor
K_b	correction factor depending on the rudder's span-wise location
K'	rudder effectiveness parameter
l	winglet chord length
l_r	winglet rudder chord length
M	surface bending moment
N	total yaw moment
N_{BWB}	yaw moment of BWB configuration due to sideslip angle β
$N_{crocodile\ flaps}$	yaw moment from deflected crocodile flaps
N_{OEI}	yaw moment generated by inoperative engine due to the wind-milling effect
N_{OEO}	yaw moment generated by operative engine at maximum thrust
$N_{winglet}$	yaw moment generated by winglet rudder deflection
OEI	one engine inoperative
p	resulting static aerodynamic pressure on the morphing trailing edge
$\bar{p}_{cf}$	mean static pressure on the crocodile flap
$\bar{p}_{nom}$	wing loading
$\bar{p}_{ref}$	mean static pressure/reference pressure
q	dynamic pressure
$y_{ac,cf}$	Y-position of aerodynamic centre of deflected crocodile flaps
y_{cf}	Y-distance between BWB centre-line and aerodynamic centre of deflected crocodile flap
y_e	Y-distance between BWB centre-line and engine centre-line
x	chord coordinate
$x_{ac,winglet}$	X-position of winglet's aerodynamic centre
x_{cg}	X-position of BWB's centre of gravity
$x_{winglet}$	X-distance between winglet's aerodynamic centre and BWB's CG position
β	sideslip angle
δ_{cf}	crocodile flap deflection angle
$\delta_{winglet}$	winglet rudder deflection angle
η	overall flap deflection angle for the aileron mode
η_{upper}, η_{lower}	deflection angle of the upper flap, deflection angle of the lower flap